Sunlight-activated photocatalytic efficiency of novel Zr-CoS-PTh composite for superior wastewater remediation

A. Naseem [a], N. Nadeem [a], S. Noreen [a], M.S. Youssef [b], Z. A. Rehan [c], H. T. Ali [b], G. Mustafa [d], M. Zahid [a,*]

[a] *Department of Chemistry, University of Agriculture, Faisalabad- 38040 Pakistan*

[b] *Department of Mechanical Engineering, College of Engineering, Taif University, Kingdom of Saudi Arabia*

[c] *Department of Chemistry, College of Science, Sultan Qaboos University Al-Khoud-123, Oman*

[d] *Department of Chemistry, University of Okara, Okara Pakistan*

This research aimed to develop novel Zr-CoS-PTh nanocomposite as photocatalyst for degradation of RhB dye. The Zr-CoS-PTh nanocomposite was synthesized via a hydrothermal method and was characterized using FTIR, XRD, and SEM/EDS. The composite achieved up to 98% dye degradation within 90 minutes under optimized experimental parameter such as pH 7, H_2O_2 concentration of 5 mM, catalyst dosage of 30 mg/100 mL, and dye concentration of 50 ppm. The optimization of the experimental parameters was also studied Response Surface Methodology (RSM). The kinetic analysis showed that 1st order supports the reaction mechanism. Scavenger analysis revealed that hydroxyl radicals, photogenerated holes, and superoxide radicals played pivotal roles in the photocatalytic degradation process.

(Received June 30, 2025; Accepted September 11, 2025)

Keywords: Cobalt sulphide, Sunlight-driven photocatalyst, Nanocomposite, Polythiophene composite, Photocatalyst

1. Introduction

Environmental pollution is a critical global challenge that worsens annually, causing significant and irreversible harm to the planet. Water pollution is generated by organic pollutants from industries such as textiles, medicines, paper, and leather [1, 2]. Methylene blue (MB) is commonly applied in the coloration of cotton and silk fabrics [3]. Around 10-15% of the applied dye is discharged into the wastewater during the dyeing process [4]. When released into water bodies, these dyes can block sunlight and impart vibrant colors that induce toxicity in fishes and destroy food webs. About 200,000 tons of dye-contaminated water are emitted in effluents each year [5]. Pigments, pesticides metal like Cr(VI) in water can work as mutagens and carcinogens [6]. There is a need for an efficient and environmentally friendly alternative for wastewater treatment that utilizes sunlight to address a wide range of contaminants by producing harmless byproducts.

Because of their chemical and thermal stability, conventional methods—such as basic physical, chemical, and biological treatments—are often ineffective in breaking down highly colored effluents [7]. The development of advanced oxidation processes (AOPs) has gained prominence due to the nonselective degradation potential of reactive radicals [8, 9]. The mobility of electrons and the presence of holes acilitates the generation of reactive species like hydroxyl radicals ($^{\bullet}OH$) and superoxide ions ($O_2^{\bullet-}$), which cause the degradation of pollutants and convert them into CO_2 and H_2O [10]. These charge carriers are significant in redox reactions that lead to the photocatalytic degradation of toxic pigments in water [1, 11].

* Corresponding author: rmzahid@uaf.edu.pk
https://doi.org/10.15251/JOR.2025.215.565

The role of polythiophene as an excellent support in a heterojunction with cobalt sulfide is linked with its band gap. Due to the small band gap (around 2.0 eV), UV and visible light can drive an electron from the VB to the CB. The conjugated polymer structure of polythiophene provides a conductive matrix with delocalized π-electrons, creating an ideal environment for efficient charge transport [12]. In the heterojunction with cobalt sulfide, these π-electrons can facilitate electron transfer to cobalt sulfide, enhancing its catalytic activity. The synergistic interaction between polythiophene and cobalt sulfide-zirconium in the photocatalyst increases the excitation of electrons upon absorbing visible light possessing energy equal or exceeding to the band gap [13].

Semiconductor-based photocatalysis is an affordable, sustainable, environmentally friendly, and safe method that supports applications including CO_2 reduction, water splitting, and the removal of organic pollutant [11]. Polythiophene's inherent stability ensures durability in the composite structure, supporting long-term environmental and thermal stability[14]. The polythiophene/cobalt sulfide heterojunction exhibits superior methylene dye degradation properties.

Metal suphides are among the promising candidates for sustainable environmental remediation [15]. Cobalt sulfide (CoS), a prominent member of metal dichalcogenides, emerges as an exceptional heterogeneous semiconductor with distinctive properties for wastewater treatment. CoS exhibits tunable band gap, making it suitable for advanced oxidation processes. Its band gap, a crucial determinant of semiconductor efficiency, aligns optimally with the visible light spectrum, ensuring effective utilization of solar irradiation for photocatalysis. Most single-component photocatalysts have poor photocatalytic activity due to weak spectrum absorption, rapid recombination of the photogenerated charge carrier, and insufficient active sites. When coupled with polythiophene, the synergistic effect of their heterojunction further enhances the photocatalytic performance [16, 17].

As a conductive polymer, polythiophene facilitates efficient charge separation and transport, addressing a common limitation in semiconductor-based photocatalysts [18]. The interplay between polythiophene and CoS-Zr facilitates the production of reactive species, making the composite highly effective for degrading methylene blue in wastewater.

In this research, the novel ternary nanocomposite, i.e., Zr-CoS-PTh, is fabricated using a hydrothermal approach. It demonstrated an increased photocatalytic activity due to improved charge carrier separation at the Zr-CoS and PTh interfaces in a ternary heterojunction. The novel Zr-CoS-PTh nanocomposite was fabricated by facile hydrothermal treatment. It was well characterized by FTIR, XRD, and SEM/EDS, confirming the catalyst's crystallinity, functionality, and surface morphology. The high crystallinity and perfect phase analysis, well-identified functional groups, and morphological details of the composite photocatalyst confirmed the successful synthesis. The developed heterojunction performed well for photocatalytic dye degradation. The identification of key radical scavengers helps in proposing a degradation mechanism. The kinetic analysis was performed with 1st and 2nd order models. The validity of the experimental procedure was checked using the Response Surface Methodology (RSM) statistical results.

2. Materials and methods

2.1. Chemicals

Anhydrous Ferric chloride ($FeCl_3$, 97 %), Chloroform ($CHCl_3$, 95 %), Cobalt chloride hexahydrate ($CoCl_2$. $6H_2O$, 98%), Thiourea (H_2NCSNH_2, 98n%), Ammonia (NH_3, 98%), Zirconium chloride ($ZrCl_4$,96 %), Acetone (CH_3COCH_3, 95 %), Ethanol (C_2H_5OH, 95 %). Sodium hydroxide (pellets, 98 %) and Hydrochloric acid (35 % w/w) were obtained from Sigma Aldrich. Distilled water was used for all experimental work.

2.2. Synthesis of polythiophene (PTh)

Polythiophene was prepared through a conventional chemical oxidation. Anhydrous $FeCl_3$ was used as an oxidizing agent during the normal chemical oxidation method to create polythiophene, with no post-doping steps. For this purpose, chloroform ($CHCl_3$) (80 mL) was added to the thiophene monomer (2 mL) in the three-necked round-bottom flask. The thiophene solution

was combined with the freshly prepared (9 g) anhydrous $FeCl_3$ solution in chloroform while being vigorously stirred. The precipitation of a black hue confirmed the polymerization of thiophene. With constant stirring, the polymerization continued for a set amount of time. A dark brownish filtrate was produced after filtration and washing. The PTh was then dried for 24 h in a vacuum [19].

2.3. Synthesis of cobalt sulphide (CoS):

The hydrothermal treatment approach was used to fabricate CoS. The salt precursors of $CoCl_2.6H_2O$ (1.9 g) and thiourea (0.9 g) were mixed in 25 ml of distilled water. Then ammonia solution (75 ml) was added under constant stirring to homogenize the constituents. Distilled water (200 ml) was added to the solution. It was placed in a stainless-steel Teflon-lined autoclave reactor at 423 K for 12 h. The resulting precipitates were thoroughly washed using distilled water/ethanol, followed by vacuum filtration and drying at 373 K for 24 h.

2.4. Synthesis of Zr-CoS-PTh and Zr-CoS

In a typical synthesis of the composite (Zr-CoS-PTh), in situ hydrothermal approach was utilized. For this case, polythiophene was dispersed into (500 mL) deionized water using ultrasonication to achieve dispersion. After stirring (polythiophene/water), the suspension was combined with Cobalt chloride (1.9 g), thiourea (0.9 g), and ammonia solution (75 mL). The result was a clear suspension. After continuous stirring, a small percentage of zirconium chloride ($ZrCl_4$) was added to the solution. This was then transferred to the autoclave for 12 h at 423 K. After that, it was washed before being dried at 373 Kelvin for 24 h. For the synthesis of Zr-CoS, same process was opted except the addition of polythiophene (PTh).

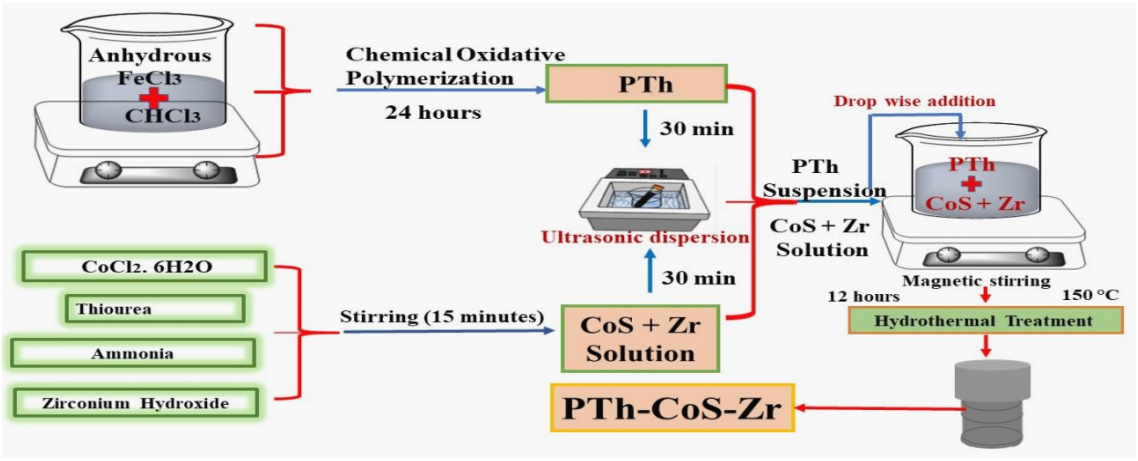

Fig. 1. Shows synthesis of ternary composite (PTh/CoS/Zr) and binary composite (CoS/Zr).

2.5. Characterization

The crystal structure of the catalysts was examined using X-ray diffraction (XRD, Rigaku) with Cu-Kα radiation (λ = 0.154056 nm), operating at 45 kV and 40 mA. Functional groups present on the catalyst surfaces were identified through Fourier-transform infrared (FTIR) spectroscopy (PerkinElmer Spectrum 100). Morphology and elemental composition were characterized using a SEM (JSM-7000F, ACCEL VOLT 10.0), EDS, respectively. This includes confirming the structure and composition of the ternary composite developed for best results in water remediation. The absorbance of treated and untreated samples was measure using UV-Vis spectrophotometer (CECIL CE 7200).

2.6. Photocatalytic dye degradation

The photocatalytic degradation efficiency of the photocatalyst was assessed under natural sunlight. Typically, 100 ml of dye solution was taken in a beaker, and a given amount of

photocatalyst was added. After sonication for a few seconds, the beakers were placed in the dark for 30 minutes. The ultrasonication treatment helps in the efficient dispersion of photocatalysts, and improved interactions among pollutants and photocatalysts can be achieved. After 30 minutes, the given oxidant amount was added, and placed under sunlight in an orbital shaker. After the completion of the reaction for a particular time, the breakers were removed from sunlight, the aliquots were separated from the photocatalyst, and their absorbance was determined using a spectrophotometer. The percentage degradation of dye was computed using the formula given below[20]:

$$Degradation\ (\%) = (1 - \frac{C_t}{C_0}) \times 100 \quad (1)$$

Here C_0 and C_t are the dye concentrations (the initial and at a given time, respectively).

3. Results and discussions

3.1. FTIR analysis

The surface functional group identification of Zr-CoS and Zr-CoS-PTh composite was determined using FTIR and the results obtained are presented in Figure 2(a). Transmittance maxima are found at 705 cm^{-1}, 1510 cm^{-1}, 2900 cm^{-1}, 3420.89 cm^{-1}, and 1223 cm^{-1} . FTIR spectra of Zr-CoS-PTh exhibits an elongated broadband at 850 cm^{-1} owing to Co-S bond stretching vibrations. The tiny transmittance peak at 2900 cm^{-1} is ascribed to the vibration mode of C-H. The signal at 705 cm^{-1} indicates stretching vibrations from C-H bonds within deformed clusters in ternary heterojunction. Carbon linkage with hydrogen confirms the presence of PTh in ternary composites, as evidenced by the peak at 2900 cm^{-1}. Because of low Zirconium concentration in the composites, no new transmittance peaks were identified [21].

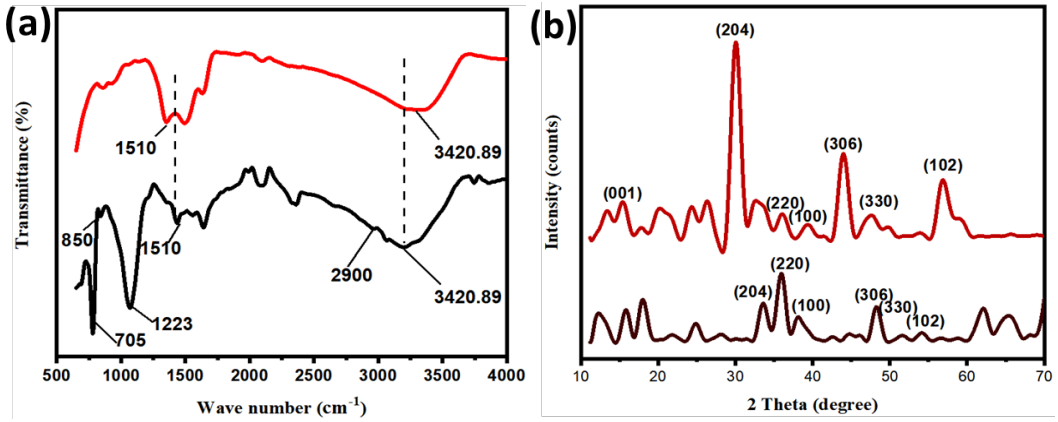

Fig. 2. FTIR analysis of (a) binary composite (CoS/Zr) and (b) ternary composite (PTh/CoS/Zr).

3.2. XRD analysis

The XRD spectrum was shown in Figure 2(b). The broad peak around 20° is for polythiophene, indicating its amorphous characteristics, particularly along the (001) plane. The PTh-CoS-Zr composite displays an additional peak at 30.46°, which is linked to the incorporation of dopants within the polythiophene matrix [22]. This shift suggests structural modifications due to the embedding of CoS-Zr into the polymer backbone, confirming successful doping. XRD analysis of CoS nanoparticles reveal a hexagonal shape with diffraction peaks of (111), (200), (311), (222), (331), (511), (440) and (531) planes at 2θ of 15.5°, 17.8°, 29.9°, 31.4°, 39.5°, 47.8°, 52.5° and 54.9° respectively (JCPDS Card file No. 68-6801) [23]. Two discrete peaks at 29.8° and 30.8° represent

the CoS phase (JCPDS card no. 65-1765) [24].The XRD pattern of Zr nanoparticles reveals a distinct peak at 2θ values of 47.23° and 61.31° planes [25] corresponding to the (022) and (13) reflections [26].

The Scherrer equation was used to determine the average crystallite size of both binary and ternary nanocomposites [27]:

$$D = K\lambda/\beta \cos\theta \quad (2)$$

D corresponds to the crystallite size, K represents the Scherrer constant (0.94), λ is the X-ray wavelength (0.154 nm), β is the full width at half maximum, and θ is the diffraction angle. CoS-Zr and PTh-CoS-Zr crystallites were estimated to have an average size of 4.6 nm and 5.5 nm. The increment in the size may be attributed to the inclusion of PTh in the ternary composite.

3.3. SEM-EDS analysis

SEM-EDS is a technique that allows for morphological characterisation and investigation of surfaces, both organic and inorganic. The SEM images and EDX pristine and ternary nanocomposite are shown in Figure 3. The sheet-like shape of polythiophene (PTh) with crumpled edges demonstrated the exfoliation of PTh during the oxidation process.

PTh doping resulted in significant modifications in ternary CoS-Zr-PTh structure. After adding PTh, the ternary hybrid crystallized and grew evenly, with CoS nanorods anchored over Zr layers and wrinkled PTh sheets. CoS exhibits a flower like structure [28]. PTh doping of CoS-Zr composite in CoS-Zr-PTh may cause differences in the morphology of CoS nanorods. PTh-doping has significantly altered the morphology of nanorods. Additionally, their size and consistency have been impacted. PTh doping has significantly reduced agglomeration, resulting in homogeneity in CoS-Zr nanorods.

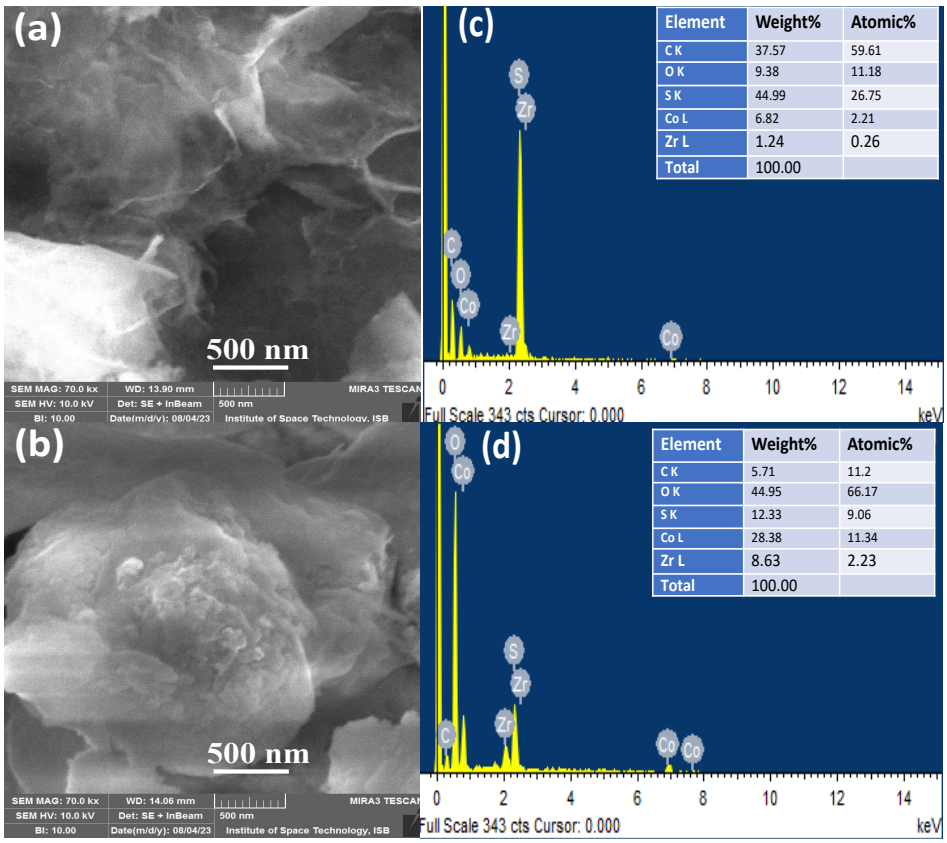

Fig. 3. SEM-EDS analysis of (a,c) ternary composite (PTh/CoS/Zr) and (b,d) binary composite (CoS/Zr).

3.4. Effect of multiple factors on dye degradation

3.4.1. Effect of pH

The pH value is an important variable that affects the charge characteristics of the substrate in the photocatalytic process. At several pH ranges from 2 to 9, the photocatalytic activity of CoS/pth/Zr was detected while other values were held constant. The maximum degradation of 80% was seen for binary (CoS-Zr) and 90% for ternary (CoS-Zr-PTh) nanocomposites at pH 7 as shown in Figure 4(a). Since MB is a cationic dye, maximal dye degrading was shown at pH 7, where more methylene blue dye molecules were immobilized on the substrate of the catalyst as the solution's pH rose. When the pH was acidic, the photocatalyst's positive charge prevented cationic species from adhering to it; however, as the pH changed from acidic to basic, the surface acquired a negatively charged, and the cationic dye was drawn to this negative surface as a result of the electrostatic interaction between cationic and anionic species[29].

3.4.2. Effect of catalytic dose

The catalyst doses varying between 10 and 50 mg per 100 ml were used. At higher initial dye concentrations, reaching up to 30 mg per 100 ml, the percentage degradation of MB increased. However, further increases in catalyst dosage resulted in a gradual decrease in degradation efficiency. The increased-degradation efficiency by increasing catalyst conc. is attributed to the greater surface area and more active sites, thereby enhancing the dye molecules degradation [30]. Both CoS-Zr-PTh and CoS-Zr showed maximum degradation of 90% and 80% at 30 mg/100 ml. Parallel to this, when the composite dosage is raised over its ideal level (30 mg/100 ml), particle clumping may occur, making the reaction mixture murky. As a consequence, less light was absorbed by the earth for dye removal, and the phenomenon was limited as a result of illumination dispersion across the area of agglomerated particles. As a result, the degradation rate dropped as the catalytic dosage was increased above the optimal threshold. The effect of catalyst dose is shown in Figure 4(b).

3.4.3. Effect of oxidant dose

Since hydroxyl radicals are a crucial component in the photodegradation process, their production has an impact on how well materials degrade. Oxidants like H_2O_2, HSO_5^-, SO_3^{2-}, and $S_2O_8^{2-}$ are required for the AOP. Numerous studies indicate that pollutant removal occurs rapidly at the initial stage but slows down over time due to excessive scavenging and light attenuation. H_2O_2 is crucial for the hydroxyl radical's production in the Fenton reaction (OH). Variable amounts of H_2O_2 were extracted from the reaction medium at concentrations of 5, 10, 15, 20, 25, 30, and 35 mM to study the impact of oxidants on dye degradation. It was shown that degradation increased with increasing oxidant dosage and peaked at 5 mM hydrochloric acid in Error! Reference source not found.(c)**.** It showed a 90% peak value for ternary and 80% for binary composite at 5 mM. The breakdown of H_2O_2 under sunlight is thought to be the cause of this behavior, which results in the creation of very active hydroxyl radicals (OH). The effectiveness of degradation was improved, but only to a certain point, as the number of hydroxyl radicals rose along with the dose of oxidants. Both binary (CoS-Zr) and ternary (CoS-Zr-PTh) nanocomposites performed maximum degradation at 5 mM oxidant dosage.

3.4.4. Effect of irradiation time

The starting dye concentration, pH, oxidant, and catalytic dose were all kept at their optimal values and the illumination period for the MB dye was chosen from 10 to 90 minutes. After 10 minutes, the absorbance of the mixture exposed to the sunlight was determined using a "spectrophotometer". The amount of degradation began to rise with time, reaching its peak (90% for ternary and 80% for binary composite) at 90 minutes. To obtain the best performance of MB dye degradation utilizing CoS/Pth /Zr and CoS/Zr as a composite photocatalyst, 90 min was chosen as the ideal period as shown in Figure 4 (e).

3.4.5. Effect of initial dye concentration

By bringing variation in concentration from 10 to 60 ppm while keeping the pH, catalytic, and oxidant dose constant, the impact of the dye amount on dissolution rate was found. It was discovered that, at a particular amount (50 ppm), the degradation is maximum as shown in Figure 4(d). When the response mixture's solution concentration was more than 50 ppm, the degradation efficiency rapidly declined even when the initial concentration rose. As the dye concentration increases beyond the optimum value (50ppm), the direction of incident photons in the mixture also decreases. When the appropriate amount of MB dye is raised during constant luminance, it results in a minimal photon number being captured by the catalyst. The catalysts exhibit degradation values of 90 % (ternary) and 80 % (binary) dye concentration at 50 ppm.

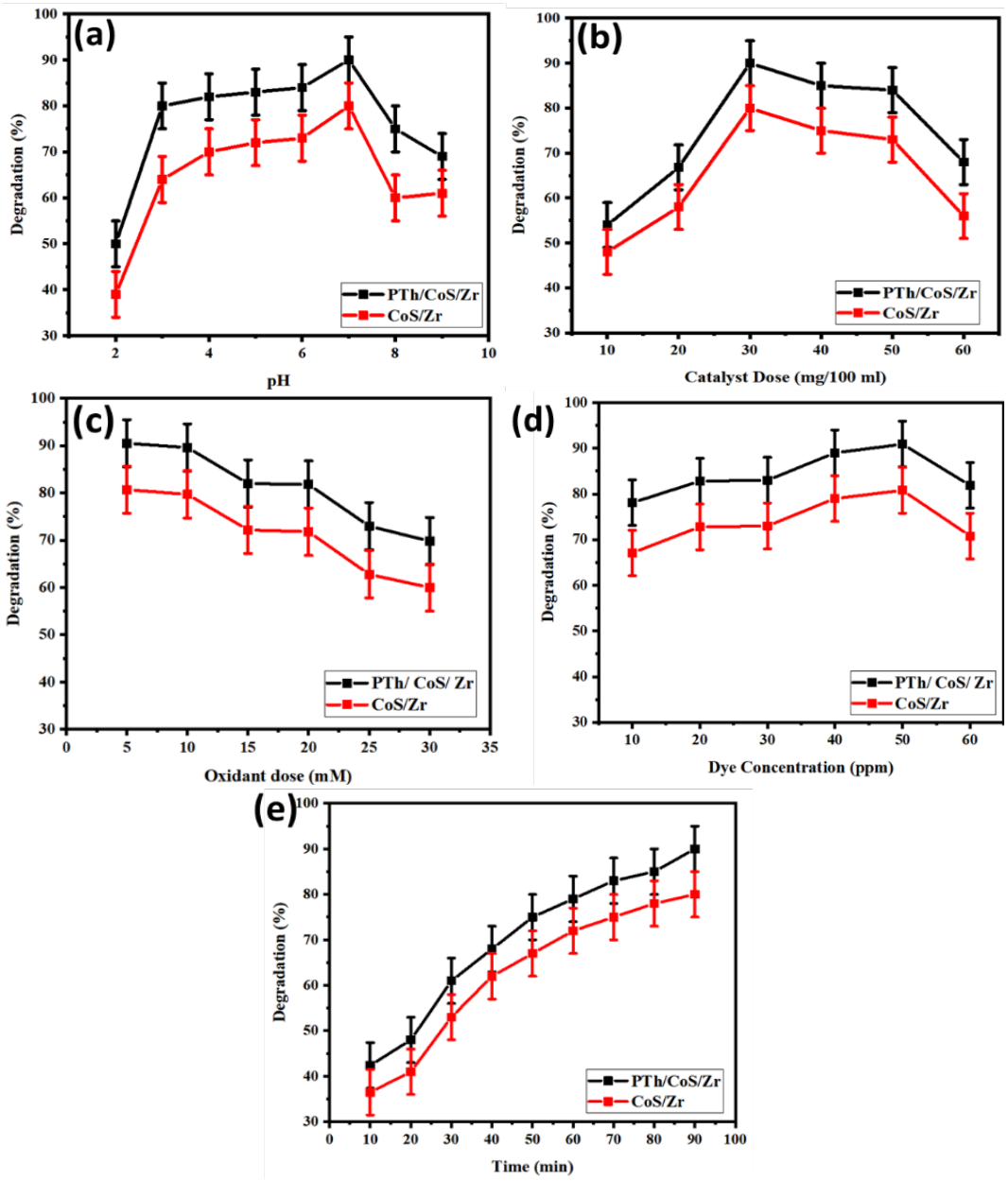

Fig. 4. Optimization of influencing factors (a) pH, (b) irradiation time, (c) catalyst dose, (d) dye concentration, (e) oxidant dose.

3.4.6. Reusability study

The reusability potential of catalysts must be assessed to determine their realistic environmental uses and economic sustainability. As a result, reusability tests of nanoparticles were conducted across five consecutive runs. The reusability of the catalysts was checked for up to 5 cycles. The reaction mixtures were kept in direct sunlight using optimized reaction conditions i.e., pH = 7, catalytic dosage = 30 mg/100 mL, initial dye concentration (IDC = 50 ppm), and reaction time of 90 minutes for all catalysts. Upon completion of the reaction, the dye solution was collected and centrifuged to separate the catalysts. The catalyst was rinsed thoroughly with deionized water, oven-dried for subsequent reuse for later cycles. The results demonstrated a very small decreease in MB degradation even after the 5th run using both (CoS-Zr) and ternary (CoS-Zr-PTh) photocatalysts. The reusability investigation revealed that these catalysts can be reused efficiently up to five times (Figure 5a).

3.4.7. Scavenging study

In this study, scavenging experiments were performed to identify the primary radicals involved in dye degradation. The radical scavengers used in this study were potassium dichromate ($K_2Cr_2O_7$), DMSO, EDTA, and ascorbic acid, used to scavenge electrons, hydroxyl radicals, holes, and superoxide anion radicals, respectively. The 5 mM concentration of all scavengers was added into a reaction mixture under optimized conditions of time, pH, catalyst dose, oxidant does etc,.

The influence of several scavengers on MB degradation using CoS-Zr-PTh and CoS-Zr is shown in Figure 5(b). Besides, EDTA, DMSO, Ascorbic acid, and $K_2Cr_2O_7$ reduced degradation from 90 % to 47 %, 50 %, and 68 % for CoS-Zr-PTh and from 80 % to 38 %, 57 % for CoS/Zr, suggesting that holes, hydroxyl radicals, and superoxide radicals played crucial roles in the degradation mechanisms of both catalysts.

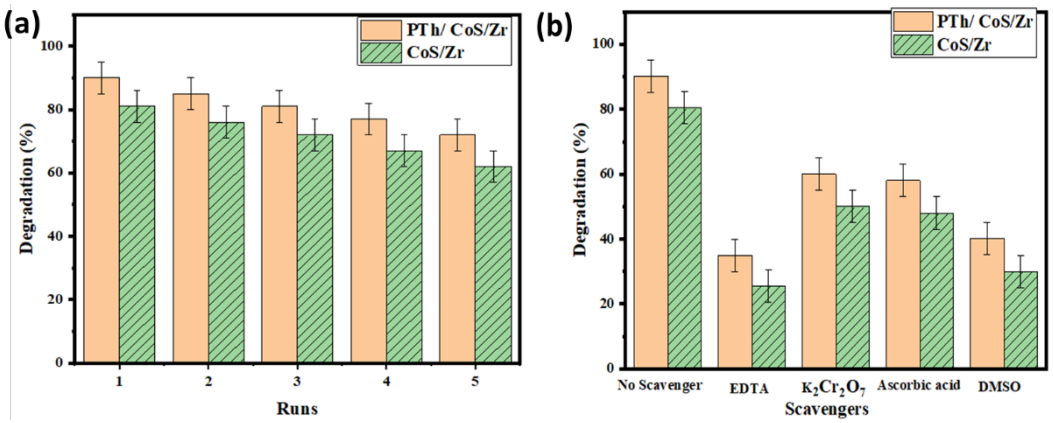

Fig. 5. (a)Reusability experiment of ternary and binary composites (b)Scavengers experiment of ternary and binary composites.

3.4.8. Mechanism of photocatalytic degradation

Catalysts and light are used for the acceleration of heterogeneous photocatalysis, which is responsible for the organic pollutant degradation and Dyes (Slama et al., 2021). After light absorption, the electrons jump from valence band (VB) to the conduction band (CB) and the resulting holes in the VB generate reactive hydroxyl radicals that contribute to pollutant degradation. The oxidizing species superoxide is formed by the redox reaction of photo-excited electrons with oxygen. The whole mechanism of degradation is shown in Figure 6.

$$\text{Semiconductor} + hv \rightarrow \text{Semiconductor} (e^-_{CB} + h^+_{VB})$$

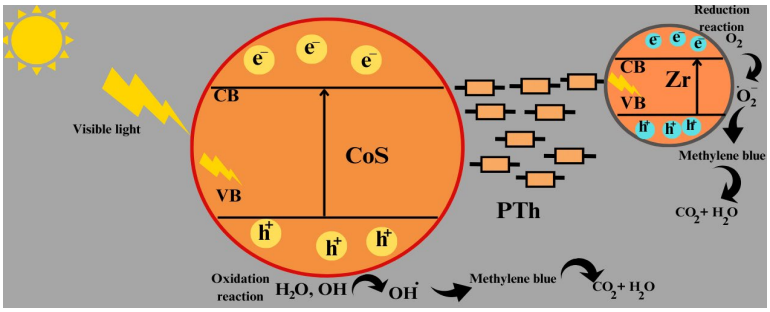

Fig. 6. Proposed photocatalytic degradation mechanism of MB dye using CoS-Zr/PTh composite.

By absorption of photons of energy that is higher than the bandgap energy of the semiconductor, e^- are excited from the VB to the CB. The reducing holes in VB transfer at the surface of the photocatalyst generate hydroxyl radical, that can be used for pollutant degradation. The oxidizing species, superoxide, are formed by the redox reaction of photo-excited electrons with oxygen.

$$\text{Semiconductor} + hv \rightarrow \text{Semiconductor} (e^-_{CB} + h^+_{VB})$$

In case of polymers, polythiophene, polyaniline, and polypyrrole have a strong potential for the process of photocatalysis[31]. The categories of conducting polymers into "n-type" and "p-type" relies on the motion of their charge carriers. The "electron-rich" conducting polymers have the potential to conduct "holes", so they are considered p-type semiconductors. Furthermore, the p-type can make "p-p type heterojunction" by adding other p-type as dopant ("CoS, NiO, V_2O_5, $ZnFe_2O_4$"). When doped with n-type particles, "p-n heterojunction" results ("ZnO, TiO_2, WO_3".

Cobalt sulfides are attractive among the metal chalcogenides due to their distinctive catalytic, electrical, electrochemical, and optical properties. Cobalt sulfide can be found in a variety of metal chalcogenide phases (including CoS, CoS_2, Co_3S_4, and Co_9S_8) and is difficult due to its chemical makeup. It also has a substantial inherent absorption in the visible electromagnetic spectrum.

Heterogeneous photocatalysis clears the aquatic environment of contaminants by producing momentary hydroxyl radicals. By using hydroxyl radicals, organic pollutants are removed, and the byproducts are converted into mineral components or less harmful organic molecules. Zinc oxide, Iron (III) oxide, tungsten trioxide, vanadium oxide, titanium dioxide, and niobium pentoxide are utilized as successful photocatalysts in photocatalytic water treatment. Such systems have a number of benefits over conventional thermal catalysis, including (1) The utilization of solar light, a renewable resource, and (2) High reaction speeds with low energy use. (3) Lesser reactivity circumstances. Most contemporary oxidation processes occur in aqueous solutions, where adsorbed water molecules are oxidized to form reactive hydroxyl radicals at the catalyst surface.

3.5. Kinetics study

The degradation of MB by ternary CoS-Zr-PTh and binary CoS-Zr nanocomposites was investigated using 1st and 2nd-order kinetic models.

$$1^{st}\text{-order kinetics:} \quad \ln C_O/C_t = k_1 t \tag{3}$$

$$2^{nd}\text{-order kinetics:} \quad \frac{1}{C_T} - \frac{1}{C_O} = k_2 t \tag{4}$$

The graph between $1/C_t$-$1/C_o$ and the time of irradiation is illustrated by a straight line as seen in Figure 7. The findings show that MB degradation by a ternary CoS-Zr-PTh nanocomposite follows first-order kinetics. When $1/C_t$-$1/C_o$ is plotted against time, a straight line forms and the linear regression slope equals (k), which is the second-order apparent rate constant. CoS-Zr-PTh has higher rate constants k, indicating more efficiency in sunlight compared to its equivalents. Second-order reaction kinetics best fit the polythiophene-based nanocomposites. R^2 values for the first-order reaction ternary CoS-Zr-PTh and binary CoS-Zr are 0.98 and 0.97, respectively, suggesting that both hybrids successfully follow the second-order reaction. These values are higher as compared to the values obtained by following a first-order reaction.

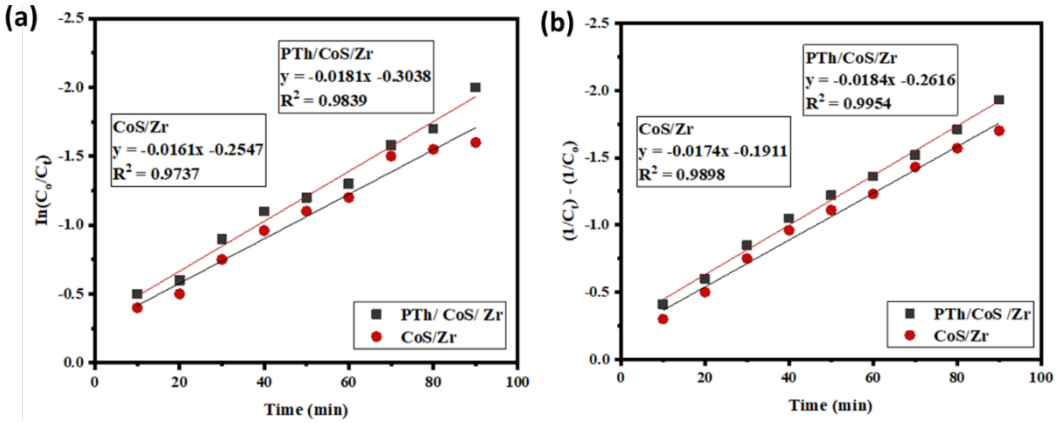

Fig. 7. Kinetics of reaction (a)1st order reaction kinetics (b) 2nd order reaction kinetics.

3.6. Response surface methodology (RSM)

RSM is a widely used statistical technique in several experimental data sets. It is equipped with both mathematical and statistical simulations for adjusting key reaction parameters[32]. A central composite design (CCD) was used to augment several parameters for methylene blue photodegradation. The CCD model is effective in predicting responses and establishing correlations between several independent variables [33]. Batch experiments were conducted to study three operational parameters for methylene blue (MB) degradation by CoS-Zr-PTh. The CCD model of RSM was used to analyze their potential interactions. CCD analyzed the correlation of pH, time, and catalyst dosage. Design Expert 7 was used as statistical software for process optimization. After providing a range of predetermined data sets, the software offers 20 random experimental runs with various concentrations of key parameters. The potential impact of the three independent variables was investigated using ANOVA analysis. The data is represented using a quadratic model for correlation [7, 31].

$$\text{Degradation (\%)} = -20.67-0.15*A+2.00*B+1.78*C+0.03*A*B-0.003*A*C-0.003*B*C-0.15*A^2-0.01*B^2-0.02*C^2$$

In the above equation, A represents pH, B represents time, and C represents catalyst dose. The reaction coefficients, like correlation coefficients (i.e., $R^2 = 0.9603$ and adjusted $R^2 = 0.9246$) suggest a strong alignment between the experimental and expected values. This equation allows for the computation of each variable's response at the determined level. The positive values reflect the positive impact of a particular variable on the response variable, and negative values reflect the negative impact.

The R^2 of 0.9603 says that 96.03% of the total variation in degradation performance was explained by the given model. R^2 values approaching 1 indicate the model's implications. The quadratic model facilitated the determination of percentage degradation through the selection of

appropriate variables. The ANOVA indicates that the lack of fit is not significant. The rest of the statistical terms are presented in Table 1.

Table 1. ANOVA Table.

Source	**Sum of Squares**	**Df**	**Mean Square**	**F-value**	**p-value**	
Model	128.73	9	14.30	26.90	< 0.0001	significant
A-pH	0.1111	1	0.1111	0.2089	0.6574	
B-Time	8.38	1	8.38	15.77	0.0026	
C-Catalyst	0.1333	1	0.1333	0.2507	0.6274	
AB	3.46	1	3.46	6.51	0.0288	
AC	0.0300	1	0.0300	0.0564	0.8171	
BC	0.8923	1	0.8923	1.68	0.2243	
A^2	3.55	1	3.55	6.68	0.0272	
B^2	13.68	1	13.68	25.72	0.0005	
C^2	90.00	1	90.00	169.24	< 0.0001	
Residual	5.32	10	0.5318			
Lack of Fit	4.31	5	0.8619	4.27	0.0684	not significant
Pure Error	1.01	5	0.2017			
Cor Total	134.05	19				

Std. Dev	0.7292	**R^2**	0.9603
Mean	86.45	**Adjusted R^2**	0.9246
C.V. %	0.8436	**Predicted R^2**	0.7622
		Adeq Precision	14.1242

3.6.1. Parameters optimization for ternary CoS-Zr-PTh nanocomposite

The 3-D and contour plots were shown to explain the relationship among influencing parameters that affect dye degradation. Given this method, two parameters were modified within the experimental ranges while the third one remained constant. The response surface is mapped based on two variables, with the third variable kept constant. The findings demonstrated that interactions between all three mentioned parameters were significant. Figure 8a contour graphic demonstrated that increasing photocatalyst concentration and pH while keeping reaction time constant can accelerate MB degradation.

Three-dimensional surface plots illustrating MB removal by CoS-Zr-PTh were used to examine the effect of pH and catalyst dosage (while keeping initial conc. of dye as constant), showing optimal degradation at pH 7 with a catalyst dosage of 30 mg per 100 mL."As the catalyst concentration increased, MB degradation decreased as more catalyst particles occupied active sites. A pH-catalyst dosage relationship significantly influenced MB removal efficiency. Increasing pH and the catalyst (CoS-Zr-PTh) dose reduce degradation efficiency.

Figure 8(b) of the response surface diagram illustrates the interaction between time and catalyst dose, highlighting their positive impact on MB degradation. The figure illustrates that improving both parameters boosted degradation efficacy, indicating that both parameters had positive interaction effects for dye pollutant removal. The ANOVA table indicates a notable interaction between the two components, with a p-value of 0.2243. The positive interaction between time and pH is shown by Figure 8 (c). It shows that MB dye degradation increases with the increment in these factors. At pH 7 and a contact time between 80 and 90 minutes, a removal efficiency of approximately 90% was achieved. High proficiency in individual factors may result in negligible interactions, reducing the impact of these interactions.

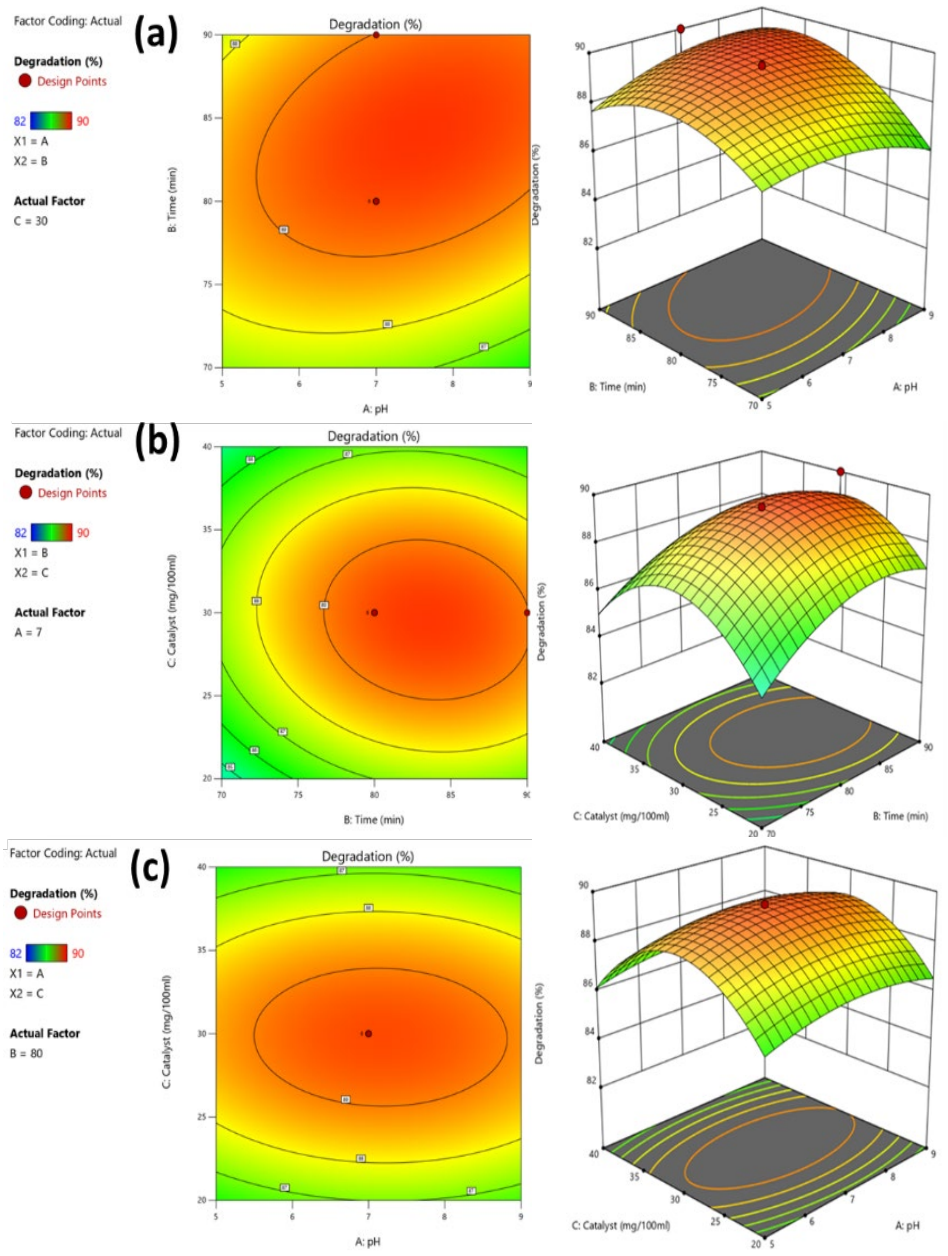

Fig. 8. Response Surface Mechanism (RSM) for the collective effect of time and pH in (a) catalyst and pH in (b) and time with catalyst in (c) time with pH.

4. Conclusion

In this study, a novel Zr-CoS-PTh ternary nanocomposite was successfully synthesized through a facile hydrothermal method, exhibiting remarkable photocatalytic performance for dye degradation. The synergistic interaction between Zr-CoS and PTh in the heterojunction structure was instrumental in enhancing charge separation, which promoted the photocatalytic degradation, achieving up to 98% degradation in just 90 minutes under optimal conditions. The XRD, FTIR, and SEM/EDS analysis confirmed the crystallinity, functionality, and morphology of the composite, further validating the success of the synthesis process. The kinetic analysis, favoring the 1st-order model with the best correlation coefficient, provided deep insights into the reaction mechanism, while the identification of radical scavengers proposed a plausible degradation pathway.

The application of Response Surface Methodology further ensured the robustness of the experimental design. These results prove Zr-CoS-PTh as a highly efficient photocatalyst for future advancements in environmental remediation technologies.

Consent for publication

All the authors agree to publish this article.

Conflict of interest

The authors declare no competing interest.

Acknowledgments

The authors would like to acknowledge Deanship of Graduate Studies and Scientific Research, Taif University for funding this work.

References

[1] Tahir, N., et al., Journal of Photochemistry and Photobiology A: Chemistry, 2023. 436: p. 114376; https://doi.org/10.1016/j.jphotochem.2022.114376
[2] Zubair, U., et al., Membranes, 2022. 12(6): p. 630; https://doi.org/10.3390/membranes12060630
[3] Chen, M.-L., et al., Journal of Colloid and Interface Science, 2023. 629: p. 409-421; https://doi.org/10.1016/j.jcis.2022.08.189
[4] Madkhali, N., et al., Results in Engineering, 2023. 17: p. 100920; https://doi.org/10.1016/j.rineng.2023.100920
[5] Oliva, J., et al., Applied Surface Science, 2018. 436: p. 739-746; https://doi.org/10.1016/j.apsusc.2017.12.084
[6] Pu, S., et al., Catalysts, 2018. 8(6): p. 251; doi: https://doi.org/10.3390/catal8060251
[7] Nadeem, N., et al., Applied Surface Science, 2021. 565: p. 150542; https://doi.org/10.1016/j.apsusc.2021.150542
[8] Ahmad, N., et al., Journal of Environmental Management, 2021. 295: p. 113362; https://doi.org/10.1016/j.jenvman.2021.113362
[9] Mehr Un, N., et al., International Journal of Environmental Science and Technology, 2024.
[10] Akhtar, N., et al., Materials Chemistry and Physics, 2024. 316: p. 129067; https://doi.org/10.1016/j.matchemphys.2024.129067
[11] Tahir, N., et al., Journal of Environmental Management, 2023. 337: p. 117706; https://doi.org/10.1016/j.jenvman.2023.117706
[12] Ansari, M.O., et al., Journal of Saudi Chemical Society, 2015. 19(5): p. 494-504; https://doi.org/10.1016/j.jscs.2015.06.004
[13] Sharma, S., et al., Polymers, 2021. 13(17): p. 2898; https://doi.org/10.3390/polym13172898
[14] Chandra, M.R., et al., Journal of Physics and Chemistry of Solids, 2017. 105: p. 99-105; https://doi.org/10.1016/j.jpcs.2017.02.014
[15] Nawaz, A., et al., Journal of Environmental Management, 2025. 373: p. 123530; https://doi.org/10.1016/j.jenvman.2024.123530
[16] Qayyum, W., et al., BMC Chemistry, 2025. 19(1): p. 86; https://doi.org/10.1186/s13065-025-01462-w
[17] Tahir, S., et al., International Journal of Environmental Science and Technology, 2025. 22(6): p. 4829-4846; https://doi.org/10.1007/s13762-024-05929-6

[18] Jiang, Q., et al., Environmental Science & Technology, 2025. 59(27): p. 14182-14192; doi: https://doi.org/10.1021/acs.est.5c06061
[19] Thanasamy, D., D. Jesuraj, V. Avadhanam, Polymer, 2019. 175: p. 32-40; https://doi.org/10.1016/j.polymer.2019.03.042
[20] Saleem, M.Z., et al., Physics and Chemistry of the Earth, Parts A/B/C, 2023. 132: p. 103506; https://doi.org/10.1016/j.pce.2023.103506
[21] Ikhlaq, U., et al., The European Physical Journal Applied Physics, 2015. 69(1): p. 10801; https://doi.org/10.1051/epjap/2014140246
[22] Chetia, R., et al., ACS Omega, 2024; https://doi.org/10.1021/acsomega.4c03184
[23] Yu, J., et al., Journal of the Electrochemical Society, 2014. 161(6): p. A996; https://doi.org/10.1149/2.053406jes
[24] Han, X., et al., Nanoscale, 2018. 10(6): p. 2735-2741; https://doi.org/10.1039/C7NR07931A
[25] Xiao, J., et al., Small, 2025: p. 2503335; doi: https://doi.org/10.1002/smll.202503335
[26] Cai, Y., et al., Separation and Purification Technology, 2025. 376: p. 134078; doi: https://doi.org/10.1016/j.seppur.2025.134078
[27] Arfa, U., et al., Polymers, 2023. 15(13): p. 2775; https://doi.org/10.3390/polym15132775
[28] Xiong, C., et al., Materials & Design, 2020. 195: p. 108942; https://doi.org/10.1016/j.matdes.2020.108942
[29] Nadeem, N., et al., International Journal of Environmental Science and Technology, 2021; https://doi.org/10.1007/s13762-021-03255-9
[30] Tabasum, A., et al., Water Science and Technology, 2020. 81(1): p. 178-189; https://doi.org/10.2166/wst.2020.098
[31] Mazhar, S., et al., Environmental Science and Pollution Research, 2022. 29(6): p. 9203-9217; https://doi.org/10.1007/s11356-021-16181-7
[32] Nadeem, N., et al., Environmental Research, 2022. 206: p. 112280; https://doi.org/10.1016/j.envres.2021.112280
[33] Ashiq, H., et al., Journal of Physics and Chemistry of Solids, 2022. 161: p. 110437; https://doi.org/10.1016/j.jpcs.2021.110437